A Quad-band power amplifier based on impedance frequency modulation

Zhiwei Zhang, Vincent Fusco, *Fellow, IEEE*, Zhiqun Cheng, *Member, IEEE*, Neil Buchanan, and Chao Gu

1

***Abstract*—This paper presents a novel method to design a multiband power amplifier. A coupler is used as the amplifier output circuit for achieving multiband impedance transformation. In order to support multiband operation, the coupler is modified with inserting a reactance to ground. Thus, the terminal impedance can be made to change with frequency. Further, realization of the desired frequencies of operation for a required PA design are obtained by combining the obtained periodical impedance trajectory and class-EFJ PA's impedance space. For validation, a quad-band power amplifier is designed and fabricated using the proposed method. Measurements show that the power amplifier can deliver output power of above 40.3 dBm, with drain efficiency of over 63% in the four frequency bands 0.5 GHz, 1.5 GHz, 2.5 GHz, and 3.5 GHz.**

***Index Terms*— Coupler, power amplifier, quad-band, terminal modulation.**

I. Introduction

With the rapid development of wireless communication, the transmission rate is getting faster and faster and current and future mobile communication often are required to support multi-band operating modes. Correspondingly, the RF front-end circuit also needs to support multi-band operation. As the key module of the transmitter, the power amplifier (PA) should have the ability to work well in multi-bands, e.g. [1-5]. Many of the publications on multi-band PAs are limited to dual-band operation [1]-[3], with T- or π-shaped dual-band matching circuits deployed [1, 2]. This approach represents a challenge when operation for more than two frequency bands is required. Therefore, components like switches, or MEMS are currently used to achieve the reconfigurable matching networks, necessary for multi-band operation, e.g. [3]-[4]. This method requires external control to switch between frequency bands. A multiband impedance inverter circuit is also developed to achieve a quad-band PA operation [5], where the implemented PA has a narrow working frequency band in each operation band, which cannot satisfy the typical bandwidth requirements of current commutations. In [6], T-section coupled lines are used to design quadband Doherty PAs. However, the impedance conversion involved is only between pure real impedances, which is obviously not conducive to the practical PA design. Recently, we presented a simple method to design dual-band PAs by using a fixed dual-band coupler [7], where the coupler can only realize the conversion between the impedance of pure resistance. Moreover, the operating frequency band and frequencies are fixed and cannot be changed due to the lack of frequency modulation components. These characteristics make the method reported in [7] not general and insufficient in practicality.

Different from the previous approaches reported in the literature, this paper develops a new method to achieve multi-band operation, which does not rely on external control, but only requires a reactively terminated coupler whose load as presented to the PA can present the desired multi-band matching requirement. The injection of reactance is used to achieve impedance frequency modulation, so that the conversion between complex impedances becomes possible. Further, combination of the coupler impedance and class-EFJ required impedance space presented in our work in [8], we can deduce available frequency bands and the corresponding impedance range for PA's multi-band operation. Moreover, the available frequency band at each band can be better than 300 MHz, which shows superior performance compared with previous works. In order to make the proposed method more promising for practical applications, throughout this paper normalized frequency is used in the derivation process, so that the proposed method can be applied to other required frequency bands as required by the PA specification. Also, periodic frequency modulation also enables the proposed method to not only achieve quad-band, but other such as dual-band and six-bands are theoretically feasible. In order to verify the effectiveness of the proposed method, a quad-band PA is designed and fabricated and experimental results provided.

II. Analysis of The Proposed Method

The coupler is used as the output circuit to transform the optimal load impedance of transistor to the practical required load at selected frequencies. In this paper, the required load is taken as the standard 50 Ω for the convenience of testing. The

Manuscript received June 16 2021; revised August 09 2021; accepted September 02, 2021. Date of publication xxxx; date of current version xxxxx. This work was supported by the National Natural Science Foundation (Grant 61871169 and Grant 91938201) and Zhejiang Provincial Natural Science Foundation (Grant LZ20F010004). *(Corresponding author: Zhiqun Cheng.)*

Zhiwei Zhang is with School of Electronics and Information, Hangzhou Dianzi University, Hangzhou 310018 China, and also with the ECIT Institute, Queen's University Belfast, Belfast BT3 9DT, U.K (e-mail: 2361051379@qq.com;).

Vincent Fusco, Neil Buchanan, and Chao Gu are with the ECIT Institute, Queen's University Belfast, Belfast BT3 9DT, U.K. (e-mail: v.fusco@ecit.qub.ac.uk; n.buchanan@ecit.qub.ac.uk; chao.gu@qub.ac.uk).

Zhiqun Cheng is with School of Electronics and Information, Hangzhou Dianzi University, Hangzhou 310018 China.(e-mail: zhiqun@hdu.edu.cn;)

schematic of the modified coupler is shown in Fig. 1. Here port 2 is connected via a reactance to ground, while port 3 is maintained open. Port 1 and port 4 are used as the input and output terminals to the PA. Port 1 is connected to the drain of transistor, and port 4 is connected to the standard 50 Ω PA load. The electrical lengths of all the four microstrip lines of the coupler are λ/4, and the characteristic impedances are Z_0, and $Z_0/\sqrt{2}$, respectively.

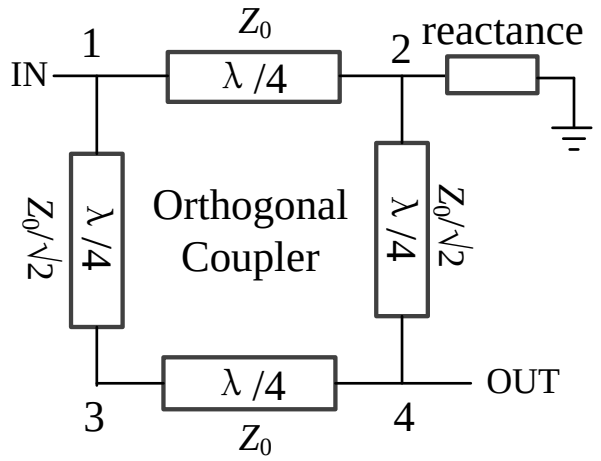

Fig. 1. Modified coupler.

The relationship between voltage and current is given by

$$\begin{bmatrix} V_1 \\ V_2 \\ V_3 \\ V_4 \end{bmatrix} = Z_0 \begin{bmatrix} 0 & +j & -j\sqrt{2} & 0 \\ +j & 0 & 0 & -j\sqrt{2} \\ -j\sqrt{2} & 0 & 0 & +j \\ 0 & -j\sqrt{2} & +j & 0 \end{bmatrix} \begin{bmatrix} I_1 \\ I_2 \\ I_3 \\ I_4 \end{bmatrix} \quad (1)$$

where the I_3=0. Z_0 is the system impedance that is equal to V_4/I_4 shown in Fig. 1.

As shown in Fig. 1, the impedance of port 2 Z_2 is obtained as

$$Z_2 = jZ_0 \tan \beta l = j\, Z_0 \tan \frac{\pi}{2} f \quad (2)$$

where β is the propagation constant. l is the physical length of this reactance. The f refers to the normalized frequency.

Based on (1) and (2),

$$V_1 = jI_2 Z_0 \quad (3)$$

$$V_4 = -j\sqrt{2} I_2 Z_0 \quad (4)$$

Then, the relationship between the impedance of port 1 Z_1 and the impedance of port 4 Z_4 is derived as

$$Z_1 = Z_4/(2 + j \tan \frac{\pi}{2} f) = \frac{Z_4\left(2 - jtan \frac{\pi}{2} f\right)}{4 + tan^2 \frac{\pi}{2} f} \quad (5)$$

The relationship expressed by (5) can be plotted in Fig. 2. Fig. 2 (a) is the real part of Z_1/Z_4, and Fig. 2 (b) is the imaginary part of Z_1/Z_4. It can be seen from Fig. 2 that both the real part and the imaginary part are periodic, and the value of period is 2 in normalized frequency.

Z_1/Z_4 is the normalized impedance and Z_4 is equal to Z_0 defined before. Therefore, we plot the normalized impedance Z_1 in the Smith chart shown in Fig. 3(a). Fig. 3(a) shows the impedance trajectory of Z_1 in two periods, that is, the normalized frequency range from 0 to 4. As shown in Fig. 3(a), the numbers inside figure (1, 3, 0, 2, 4) refer to the normalized frequency f. For example, when f=0, the impedance is 0.5+j*0. As f increases from 0 to 1, the impedance changes from 0.5+j*0 to 0+j*0, changing clockwise as shown in Fig. 3(a). Similarly, when f=1, the impedance is 0+j*0. As f increases from 1 to 2, the impedance changes from 0+j*0 to 0.5+j*0, changing clockwise as shown in Fig. 3(a). When f changes from 0 to 2, one cycle of impedance change is completed. This trend of impedance change can also be seen from Fig. 2. Because this paper considers two periods, it is natural to mark f=0,1,2, 3, 4 in Fig. 3 (a). When f changes from 2 to 4, the state of impedance change is the same as that from 0 to 2. As shown in Fig. 3(a), the red impedance trajectory represents the normalized impedance Z_1 with frequency. This trajectory is derived from (5), which means that all impedances on the trajectory can be naturally converted to 50 ohms at the corresponding frequency.

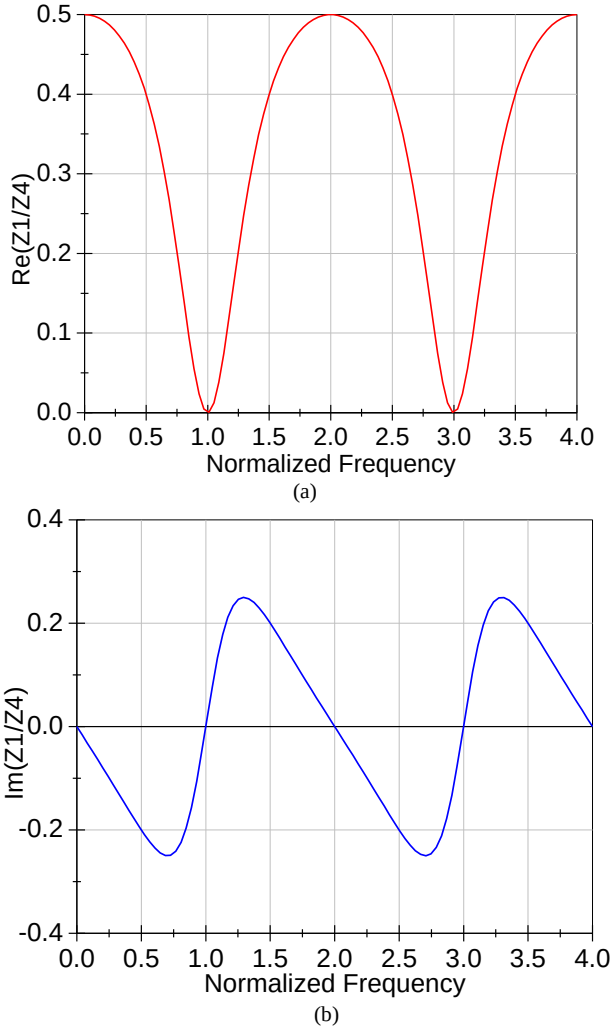

Fig. 2 The value of Z_1/Z_4 varies with the normalized frequency. (a) The real part of Z_1/Z_4. (b) The imaginary part of Z_1/Z_4.

In [8], we proposed a class-EFJ PA whose fundamental impedance is shown in Fig. 3(b). As shown in Fig. 3(b), there are several intersections between the impedance space of class-EFJ PAs and the impedance trajectory of Z_1. This yields viable normalized operating frequency bands as 0-0.6, 1.4-2.0, 2-2.6, and 3.4-4, represented by the yellow lines in Fig. 3(b). The impedances located at the yellow lines are not only load impedances expected by the class EFJ PA, but also can be naturally converted to 50 Ω at each band through the proposed coupler.

The number of concurrent bands can be adjusted by varying the number of periods. This paper only considers two periods

(0<f<4), but in fact the proposed structure is periodic (period=2), and more periods can be added as needed. In this way, not only 4 bands, but other permutations such as 2 bands, 6 bands, 8 bands, etc. can be realized by using the proposed method in this paper. Also, various actual operating frequencies can be obtained by choosing an appropriate normalized reference frequency f_r. The relationship between normalized frequency f, actual working frequencies f_a and reference frequency f_r is $f_a = f \cdot f_r$. For example, if we choose to normalize to 1 GHz, then the corresponding actual frequencies f_a are 0-0.6 GHz, 1.4-2.0 GHz, 2.0-2.6 GHz, 3.4-4.0 GHz.

Next, we can realize the transformation of the PA transistor's load impedance at available selected operating frequencies to standard 50 Ω load using the modified coupler. In this work, 0.5 GHz, 1.5 GHz, 2.5 GHz, and 3.5 GHz are selected considering current communication standards and transistor's performance. The second harmonic frequencies are 1.0 GHz, 3.0 GHz, 5.0 GHz, 7.0 GHz have impedances that are always located at the short-circuit point. In this case, the fundamental impedance and second harmonic impedance at each frequency bands are inherently converted to 50 Ω because these impedances are located on the impedance trajectory shown in Fig. 3(a). Also, these fundamental impedances are located at the class-EFJ fundamental impedance space and the second harmonic impedance are close to zero. Therefore, both fundamental impedance and second harmonic impedance are controlled well without additional operations required. This is also the advantage of the proposed modified coupler compared to the traditional matching structure.

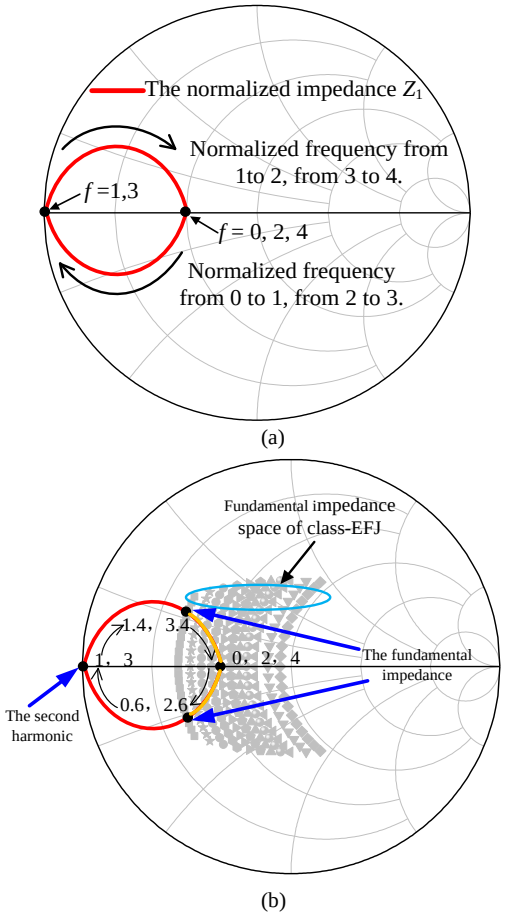

Fig. 3. (a) The normalized impedance Z_1 (normalized to 50 Ω). (b) The impedance trajectory of Z_1 in two periods and the impedance space of the class-EFJ PAs.

III. Experiments and Measurements

In order to validate the proposed method, a quad-band PA is designed and fabricated using a CGH40010F transistor, and a Rogers 4350B (ε_r = 3.66, H = 30 mil) substrate. The gate bias voltage is -2.8 V, and the drain bias voltage is 28 V for class EFJ PAs operation.

The electrical length of the inserted reactance shown in Fig. 1 can be calculated by multiplying the available normalized frequency given in Fig. 3(b) by π/2, while noting that the normalized frequency is periodic. Based on Fig. 1, we can design the modified coupler including consideration of transistor package parameters [9], which is shown in Fig. 4(a). Real-frequency technology [10] is used to synthesize the optimal coupler's impedance and electrical length values, which can be done in MATLAB or ADS. The initial value in the synthesis iteration process is shown in Fig. 1. The goal of the synthesis is that the transmission gain of the passive network is 0 dB in the four desired frequency bands. The result of this is that the electrical length of the coupler reduces from 90°to 60°. The simulated impedance of the resulting coupler design port 1 is displayed in Fig. 4(b). It can be seen from Fig. 4(b) that the simulated impedance at the I-Gen plane conforms to the theoretical value shown in Fig. 3. Also, the simulated S21 of the network is plotted in Fig. 4(c). It can be clearly seen that near 0.5 GHz, 1.5 GHz, 2.5 GHz, and 3.5 GHz, the loss of the network is small.

The input matching network is synthesized based on the broadband matching technique [11], which in this case supports frequency bands of from 0.4 GHz to 3.7 GHz. The complete schematic of the realized design is shown in Fig. 5. Fig. 6 is a photograph of the designed PA.

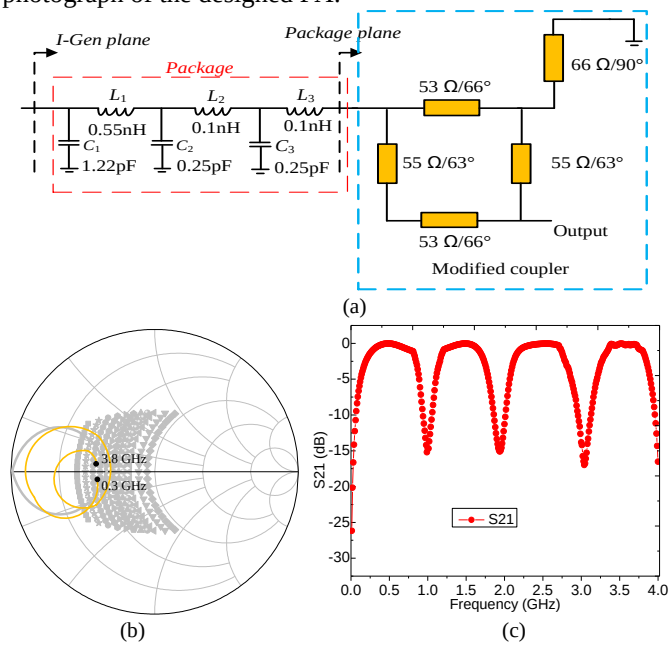

Fig. 4. (a) The designed coupler. (b) simulated impedance of this coupler (c) simulated s21.

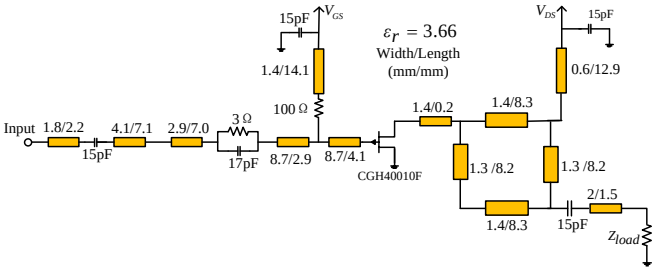

Fig. 5. The schematic of the designed PA.

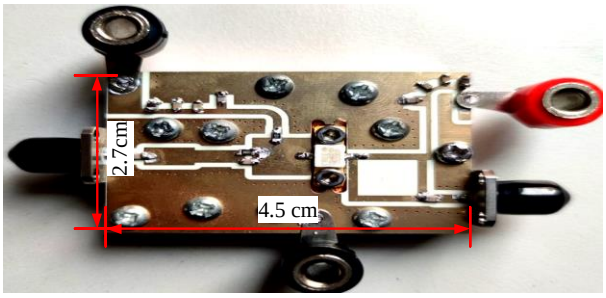

Fig. 6. Photograph of the implemented PA.

The simlulated volatge and current waveforms at several frequencies are plotted in Fig. 7. As shown in Fig. 7, these waveforms are between the class EF PA and the class J PA, validating the effectiveness of the design.

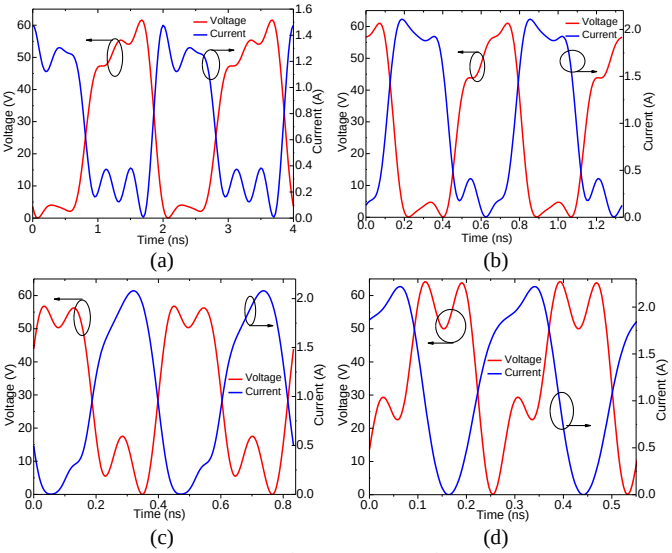

Fig. 7. Voltage and current waveforms at several frequencies (a) 0.5 GHz (b) 1.5 GHz (c) 2.5 GHz (d) 3.5GHz.

Figs. 8 (a), (b), and (c) show the measured results including gain, output power and drain efficiency. The obtained saturated output power is 40.3 dBm, 41.5 dBm, 41.3 dBm and 40.6 dBm at 0.5 GHz, 1.5 GHz, 2.5 GHz, and 3.5 GHz, respectively. Also, the measured drain efficiency reaches 64.4%, 63.6%, 65.3% and 64.3% at 0.5 GHz, 1.5 GHz, 2.5 GHz, and 3.5 GHz, respectively, with gain of over 10.7 dB in all bands. The output power at 1-dB compression point is 39.5 dBm, 38.8 dBm, 38.5 dBm and 38.6 dBm at 0.5 GHz, 1.5 GHz, 2.5 GHz, and 3.5 GHz, respectively. The measured peak PAE(power added efficiency) is 59.6%, 60.2%, 62.7% and 61.1% at 0.5 GHz, 1.5 GHz, 2.5 GHz, and 3.5 GHz, respectively.

The 5 MHz W-CDMA signal with a 6.5 dB peak-average ratio is used to drive the PA. The measured ACLR driven by this W-CDMA signal is shown in Fig. 9. The measured ACLR is smaller than -26.2 dBc with an average power of around 35.3 dBm at 0.5 GHz, 1.5 GHz, 2.5 GHz, and 3.5 GHz. The corresponding average drain efficiency is between 29.8% and 32.3%.

Several other representative PAs are listed in Table I for comparison. It can be seen from Table I that the designed PA in this paper has similar power, efficiency and gain at four frequencies compared to other PAs. However, our proposed PA has the widest available bandwidth at each frequency and the largest frequency span (between 0.5 GHz and 3.5 GHz) compared with other works. Also, in terms of design complexity it is the simplest to implement. These features demonstrate that this work provides a simple and innovative way for the design and synthesis of multi-band high efficiency PAs, while also extending the application of couplers.

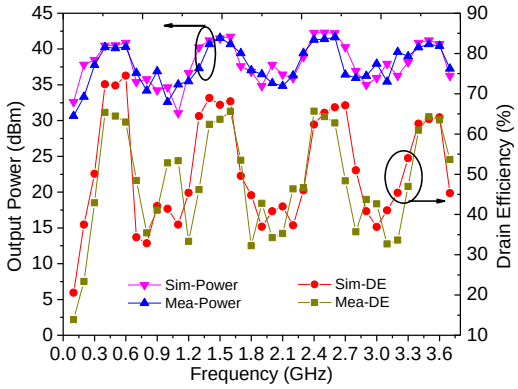

(a)

TABLE I
Performance comparison with representative PAs

Ref	Available bandwidth (MHz)	Freq.(GHz)	Power (dBm)	DE/PAE (%)	Gain (dB)	Size (cm^2)
[12]	215	0.7/0.8 1.8/2.1	41.5/39.7/ 37.7/40.7	58.2/50.3/ 48.6/56.6(PAE)	11.5/9.7/ 7.7/10.7	4.5×7.1
[13]	None	1.6/2.1 1.8/2.3	41.3/40.9 40.9/39.8	62/63/ 64/67(DE)	11/12/ 12/11	4.8×5
[14]	50	1.0/1.5 2.0/2.5	30/31 31/30	55/52/ 52/40(PAE)	9.2/8.8/ 8.0/8.1	1×3
This Work	**300**	**0.5/1.5 2.5/3.5**	**40.3/41.5/ 41.3/40.6**	**64.4/63.6/ 65.3/64.3 (DE) 59.6/60.2/ 62.7/61.1(PAE)**	**10.7/11.2/ 12.7/11.4**	**2.7×4.7**

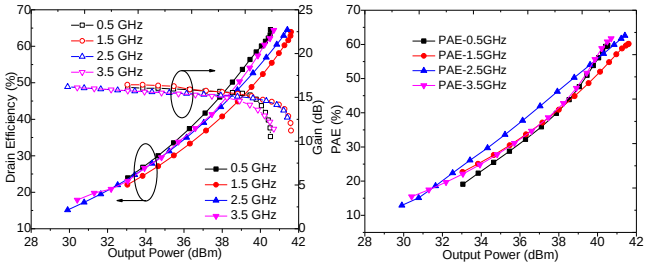

(b) (c)

Fig. 8. (a) Saturated output power, drain efficiency versus frequency. (b) measured drain efficiency, gain versus frequency output power (c) measured PAE.

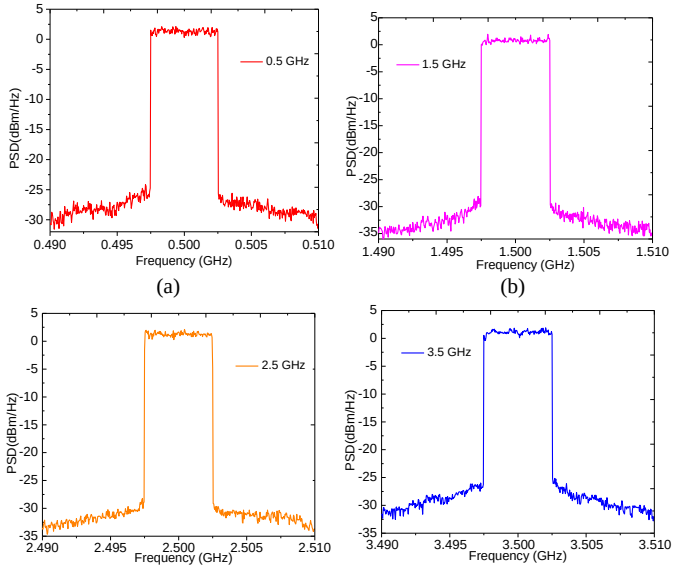

(a) (b)

(c) (d)

Fig. 9. Measured ACLR under 5MHz W-CDMA with 35.3 dBm average output power at four frequencies. (a) 0.5 GHz (b) 1.5 GHz (c) 2.5 GHz (d) 3.5 GHz.

IV. Conclusion

This paper proposes a novel method to design multi-band power amplifiers. Through insertion of a reactance, the impedance of coupler is periodically modulated with operating frequency. By combining class-EFJ PAs and the modulated impedance, the available operating frequency of PAs can be obtained. As an example, a class-EFJ PA supporting 0.5 GHz, 1.5 GHz, 2.5 GHz, and 3.5 GHz was designed, fabricated and tested. Measurements show that the PA can work well at the target frequency bands. Compared with other related work, this work shows superior performance, and design complexity is significantly reduced. These features illustrate that this paper provides a new way by which to realize quad-band power amplifiers that is more effective and simpler than previous methods.

References

[1] H. Zhang, K. J. Chen, and S. Member, "A Stub Tapped Branch-Line Coupler for Dual-Band Operations," *IEEE Microw. Wireless Compon. Lett.*, vol. 17, no. 2, pp. 106–108, Feb. 2007.

[2] Y. Wu, Y. Liu, and S. Li, "A compact Pi-structure dual band transformer," *Progress in Electrom. Research*, vol. 88, pp. 121–134, 2008.

[3] A. M. M. Mohamed, S. Boumaiza and R. R. Mansour, "Electronically Tunable Dherty Power Amplifier for Multi-Mode Multi-Band Base Stations," *IEEE Trans. Circuits Syst. I, Reg. Papers.*, vol. 61, no. 4, pp. 1229-1240, Apr. 2014.

[4] S. A. Figur, V. Ziegler, R. Quay and L. Vietzorreck, "RF MEMS variable matching networks for multi-band and multi-mode GaN power amplifiers," *2013 European Microwave Integrated Circuit Conference*, Nuremberg, 2013, pp. 324-327.

[5] X. A. Nghiem, J. Guan, T. Hone, and R. Negra, "Design of concurrent multiband Doherty power amplifiers for wireless applications," *IEEE Trans. Microw. Theory Techn.*, vol. 61, no. 12, pp. 4559–4568, Dec. 2013.

[6] X. Li, M. Helaoui, F. Ghannouchi, and W. Chen, "A Quad-Band Doherty Power Amplifier Based on T-Section Coupled Lines," *IEEE Microw. Wireless Compon. Lett.*, vol. 26, no. 6, pp. 437-439, June 2016.

[7] Z. Zhang, Z. Cheng, V. Fusco and C. Gu, "Design of a Dual-Band Power Amplifier Using a Simple Method," *IEEE Microw. Wireless Compon. Lett.*, vol. 31, no. 2, Apr. 2021.

[8] Z. Zhang, Z. Cheng, H. Ke, G. Liu and S. Li, "Design of a Broadband High Efficiency Hybrid Class EFJ Power Amplifier," *IEEE Microw. Wireless Compon. Lett.*, vol. 30, no. 4, Apr. 2020.

[9] S. Y. Zheng, Z. W. Liu, X. Y. Zhang, X. Y. Zhou, and A. W. S. Chan, "Design of Ultra-wideband High-Efficiency Extended Continuous Class-F Power Amplifier," *IEEE Trans. Ind. Electron.*, vol. 65, no. 6, June. 2018.

[10] B.S. Yarman, Design of Ultra-Wideband Power Transfer Networks via Real Frequency Techniques, Willey, UK., 2010.

[11] Z. Zhang and Z. Cheng, "A Multi-Octave Power Amplifier Based on Mixed Continuous Modes," *IEEE Access*, vol. 7, pp. 178201-178208, Dec. 2019.

[12] J. Choi et al., "Quad-band inverse class-F power amplifier using novel composite right/left-handed transmission line," in *IEEE MTT-S Int. Wireless Symp. Tech. Dig.*, 2010, pp. 1078-1081.

[13] R. Kalyan, K. Rawat, and S. K. Koul, "Design of reconfigurable concurrent dual-band power amplifiers using reconfigurable concurrent dual-band matching network," in *IEEE MTT-S Int. Wireless Symp. Tech. Dig.*, Mar. 2016, pp. 1–4.

[14] Atsushi Fukuda, Hiroshi Okazaki and Shoichi Narahashi, "A novel reconfigurable quad-band power amplifier with reconfigurable biasing network and LTCC substrates," *IEEE MTT-S Int. Wireless Symp. Tech. Dig.*, 2008, pp. 867-870.